Research Article | Vol. 5, No. 4 / 15 Apr 2026 / Optics Continuum 1184

OPTICS CONTINUUM

Amplified nonreciprocal and unidirectional reflection in a defective atomic lattice via spontaneously generated coherence

QIONG-YI XU,† CHEN PENG,† DUAN-FU CHEN, HAN-XIAO ZHANG, DONG YAN, AND HONG YANG*

School of Physics and Electronic Engineering, Hainan Normal University, Haikou 571158, China
†These authors contributed equally to this work.
*yang_hongbj@126.com

Abstract: Simultaneously realizing nonreciprocity and signal amplification in the same physical system cannot only greatly enhance the efficiency of nonreciprocal photonic devices but also facilitate their integration. We propose a scheme to achieve gain-assisted nonreciprocal or even unidirectional reflection amplification by exploring spontaneously generated coherence (SGC) activated by a weak incoherent pump in a defective atomic lattice. The numerical results show that the monochromatic to two-color nonreciprocal reflection amplification (the maximum of reflectivities $R_l \simeq 10^4$ and $R_r \simeq 10^2$), and even unidirectional reflection amplification ($R_l \simeq 10^2$ and $R_r \simeq 10^{-4}$) can be modulated freely by adjusting the relative phase ϕ, the dipole moment angle θ and the parameters of defective atomic lattice, e.g., the number and period of vacant lattice cells, the period of filled lattice cells, and so on. This indicates that nonreciprocal reflection amplification can be enhanced and modulated via the SGC effect and multiple reflections within the atomic lattice. Such efficient nonreciprocal amplification can be effectively applied to integrated chips, thereby advancing the development of quantum information technology.

1. Introduction

Optical nonreciprocity refers to the phenomenon where the transmission path's response is no longer symmetric when the source and observation points are swapped during the light propagation. This characteristic is crucial in designing nonreciprocal optical devices, such as optical isolators, circulators, and phase shifters [1–6]. These devices have boosted the development of optical signal processing, optical communication, and quantum networks [7–9]. However, optical signals may weaken or even disappear due to the interaction with the environment during propagation. The amplified nonreciprocal transmission can more efficiently protect coherent information processing against noise and backscattering benefiting from the advantages of signal amplification and optical nonreciprocity [10–13], which have attracted a great deal of research interest and demonstrated in various systems [14–16]. The physical essence is mainly based on the magneto-optical Faraday effect, optical nonlinearity, and time-reversal symmetry breaking, chiral materials, and topological photonics systems [17–23]. For instance, nonreciprocal amplification has been achieved in silicon waveguides through Brillouin scattering [24–26], active optomechanics systems [27–31], atomic systems [32–36], and parity-time (PT) symmetry systems [37,38]. It is believed that the above systems are powerful tools for the development of nonreciprocal optical amplification. However, each system has its own advantages and limitations, e.g., Faraday effect in magneto-optical medium is incompatible with integrated circuit technology, optical nonlinearity requires high power that is typically suitable for pulse systems, PT-symmetry system often requires complex external driving fields and so on. Therefore, more effective nonreciprocal optical amplification schemes need to be studied.

#592284
Journal © 2026

https://doi.org/10.1364/OPTCON.592284
Received 3 Feb 2026; revised 20 Mar 2026; accepted 21 Mar 2026; published 7 Apr 2026

Recently, we propose a scheme for engineering a unidirectional photonic reflector using a one-dimensional (1D) atomic lattice with defective cells that have been specifically designed to be vacant [39]. We further designed a coherent active atomic model with the help of microwave field to realize the amplified unidirectional broadband reflection in this 1D defective atomic lattice [40]. In our system, the defective atomic lattice has two functions: i) To break the spatial symmetry of probe susceptibility and achieve nonreciprocity; ii) The optical signal can be reflected multiple times in atomic lattices, resulting in better amplification at the gain window. It is an effective system to achieve nonreciprocal optical amplification that the combination of defective atomic lattice and active atomic model, and the different active atomic model will make the modulation of nonreciprocal optical amplification more diverse and flexible. In addition to the active atomic model of closed loop transition assisted by microwave field, the nonlinear effect caused by four-wave mixing (FWM) can amplify the probe light locating in the electromagnetically induced transparency (EIT) window [41–44], FWM process needs to satisfy momentum conservation and energy conservation, making it difficult to consider phase modulation. Another method of generating probe gain is spontaneously generated coherence (SGC) effect [45–49], which can be used for laser cooling, squeezing in resonance fluorescence, and so on [50,51], due to the destructive quantum interference between the two or more different quantum pathways [52,53]. However, it is difficult to observe experimentally. Initially, the SGC effect was observed by effectively using two sufficiently close energy levels, such as dressed-state energy levels [54–56]. Fortunately, SGC has been proved by the vacuum-induced quantum beats, that observed by the latest experiment in atomic ensembles recently [57–60]. Especially, combining the FWM and the SGC effects together can enhance the probe gain [61], and the combination of SGC and pump field can also improve the probe amplification [62,63].

In this paper, we design a scheme to check the modulation of nonreciprocal reflection amplification by the SGC effect. By using a one-dimensional defective atomic lattice to break the symmetry between left and right reflections and to provide a distributed feedback mechanism, and by combining the SGC with the pump field, we can enhance nonreciprocal reflection amplification. In this regime, for most parameters, the reflections on both sides are simultaneously either amplified or suppressed, for example, the left reflectivity can reach to 10^4 while the right reflectivity is almost 10^2. However, after optimizing the parameters, an amplified unidirectional reflection can be obtained with one-side reflectivity is enhanced to 10^2 and another side reflectivity is suppressed to 10^{-4}. It is worth emphasizing that the photonic properties of a cold-atom sample trapped in a 1D optical lattice have been studied experimentally [64,65]. Furthermore, experiments have also observed that when cold atoms are trapped in a one-dimensional optical lattice, the distributed feedback lasing effect [66] is realized through the parametric gain achieved by combining the feedback mechanism provided by the atomic lattice with the four-wave mixing effect induced by auxiliary beams. In our 1D defective atomic lattice system, vacant lattice cells are created via an experimental approach where all atoms within an optical potential well are driven out using a laser. Therefore, our scheme is feasible and has greater potential in practical applications.

2. Theoretical model and equations

As shown in Fig. 1(a), the cold ^{87}Rb atoms are driven into a three-level Lambda-type system, by a weak probe field, an incoherent pump field and a strong coupling field. The Rabi frequency (detuning) of the probe field $\Omega_p = \mathbf{E}_p \cdot \mathbf{d}_{13}/2\hbar$ $\left(\Delta_p = \omega_{31} - \omega_p\right)$ and the Rabi frequency (detuning) of the strong coupling field $\Omega_c = \mathbf{E}_c \cdot \mathbf{d}_{23}/2\hbar$ $(\Delta_c = \omega_{32} - \omega_c)$ drive the dipole allowed transitions $|1\rangle \leftrightarrow |3\rangle$ and $|2\rangle \leftrightarrow |3\rangle$ respectively. Λ represent the incoherent pump field that drives the transition $|1\rangle \leftrightarrow |3\rangle$. The matrix element $\mathbf{d}_{ij} = \langle i| \mathbf{d} |j\rangle$ is used to denote the dipole moment of transition $|i\rangle$ to $|j\rangle$. Specifically, the energy levels $|1\rangle$, $|2\rangle$, and $|3\rangle$ refer to states $\left|5S_{1/2}, F = 2, m_F = -2\right\rangle$, $\left|5S_{1/2}, F = 2, m_F = 0\right\rangle$, and $\left|5P_{1/2}, F = 1, m_F = -1\right\rangle$ of the D1 line of the cold ^{87}Rb atoms broken by static magnetic fields, respectively. In Fig. 1(b), we make each coherent field act on only one atomic transition. This means that the amplitudes $\mathbf{E}_p$ and $\mathbf{E}_c$ of the coherent field are perpendicular to the electric dipole moments $\mathbf{d}_{13}$ and $\mathbf{d}_{23}$, respectively. Where θ represents the angle between the two dipole moments $\mathbf{d}_{23}$ and $\mathbf{d}_{13}$. Next, we theoretically designed the defective atomic lattice and divided it into two periodic structural parts: part I with p_1 periods, each period consisting of a_f filled lattice cells (trapping atoms) and a_v vacant lattice cells (not trapping atoms), and part II with p_2 periods of filled lattice cells [see Fig. 1(c)]. The optical lattice is formed by a red-detuned standing-wave field of wavelength $\lambda_{Lat} = 2\lambda_0$, with λ_0 being the lattice period. Thus, the total length of 1D defective atomic lattice $L = S\lambda_0$, for $S = (a_f + a_v)p_1 + p_2$. Figure 1(d) shows the scheme of the experimental setup, which is further discussed in the Experimental feasibility section.

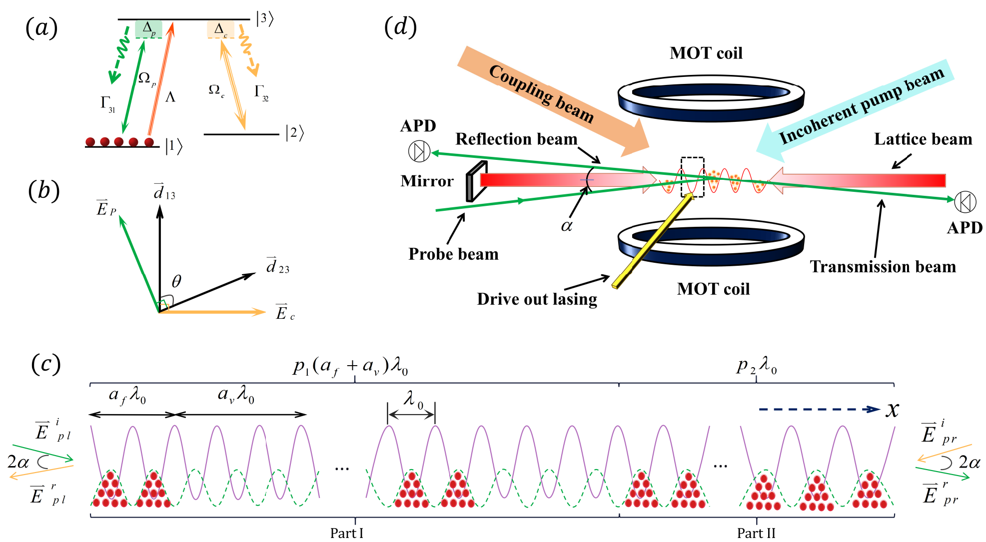

Fig. 1. (a) Energy level diagram of a three-level atomic system driven by a weak probe field, a strong coupling field, and an incoherent pump field, respectively. (b) The angular dependence between the electric field and the electric dipole moment. (c) Theoretical scheme of the 1D defective atomic lattice with the width λ_0 for each period, which comprises Part I and Part II. The probe field $\mathbf{E}_p$ is incident from either the left side (denoted by $\mathbf{E}^i_{pl}$) or the right side (denoted by $\mathbf{E}^i_{pr}$) with a small incident angle α relative to x-axis. The relevant reflected fields are denoted by $\mathbf{E}^r_{pl}$ and $\mathbf{E}^r_{pr}$. (d) The scheme of the experimental setup.

With the electric-dipole and rotating-wave approximations, the interaction Hamiltonian of atom-field can be written as follows:

$$\hat{H}_I = -\hbar \begin{bmatrix} 0 & 0 & \Omega_p^* \\ 0 & \Delta_c - \Delta_p & \Omega_c^* \\ \Omega_p & \Omega_c & -\Delta_p \end{bmatrix}. \quad (1)$$

OPTICS CONTINUUM

The density-matrix operator $\hat{\rho}$ of the atomic system is described by the Lindblad master equation in the Born-Markov approximation as follows:

$$\begin{aligned}\partial_t\hat{\rho} = &- i\left[\hat{H}_I, \hat{\rho}\right] + \Gamma_{32}\mathcal{L}\left(\hat{\sigma}_{23}\right)\hat{\rho} + \Gamma_{31}\mathcal{L}\left(\hat{\sigma}_{13}\right)\hat{\rho} + \Lambda\mathcal{L}\left(\hat{\sigma}_{31}\right)\hat{\rho} \\ &+ \gamma_{SGC}\left[\hat{\sigma}_{13}\hat{\rho}\hat{\sigma}_{23}^{\dagger} - \frac{1}{2}\left(\hat{\sigma}_{23}^{\dagger}\hat{\sigma}_{13}\hat{\rho} + \hat{\rho}\hat{\sigma}_{23}^{\dagger}\hat{\sigma}_{13}\right) + \hat{\sigma}_{23}\hat{\rho}\hat{\sigma}_{13}^{\dagger} - \frac{1}{2}\left(\hat{\sigma}_{13}^{\dagger}\hat{\sigma}_{23}\hat{\rho} + \hat{\rho}\hat{\sigma}_{13}^{\dagger}\hat{\sigma}_{23}\right)\right],\end{aligned} \tag{2}$$

the above Lindblad superoperator describes the dissipative coupling to the environment and is given by the form $\mathcal{L}\left(\hat{\sigma}\right)\hat{\rho} = \hat{\sigma}\hat{\rho}\hat{\sigma}^{\dagger} - \left(\hat{\sigma}^{\dagger}\hat{\sigma}\hat{\rho} + \hat{\rho}\hat{\sigma}^{\dagger}\hat{\sigma}\right)/2$. Here, $\gamma_{SGC} = \sqrt{\Gamma_{31}\Gamma_{32}}\cos\theta$ represents the quantum interference effect resulting from spontaneous emission from $|3\rangle \to |1\rangle$ and $|3\rangle \to |2\rangle$. The population decay rates are $\Gamma_i = \Sigma_n\Gamma_{in}$ and $\Gamma_j = \Sigma_n\Gamma_{jn}$ for $n = 1$, 2 and 3, describing inevitable dissipation. Furthermore, we make the standard transformation of the equations as follows: first, setting the initial phase of the probe, strong coupling be ϕ_p, ϕ_c respectively; then, the corresponding Rabi frequencies are defined as $\Omega_p = G_p e^{i\phi_p}$ and $\Omega_c = G_c e^{i\phi_c}$, where G_p, G_c are all real numbers; according to the definition, the density matrix element ρ_{ij} is the product of the probability amplitude of the population between states $|i\rangle$ and $|j\rangle$, and it indicates the state of coherence. Based on the discussion above, we derive the relationships: $\varrho_{ii} = \rho_{ii}$, $\varrho_{13} = \rho_{13}e^{i\phi_p}$, $\varrho_{23} = \rho_{23}e^{i\phi_c}$, and $\varrho_{12} = \rho_{12}e^{i\phi}$(where $\phi = \phi_p - \phi_c$ represents the relative phase of the two fields). Therefore, the density matrix equations [34,62] can be summarized as follows:

$$\begin{aligned}\partial_t\varrho_{11} &= \Gamma_{31}\varrho_{33} - \Lambda\varrho_{11} + iG_p\varrho_{31} - iG_p\varrho_{13}, \\ \partial_t\varrho_{22} &= \Gamma_{32}\varrho_{33} + iG_c\varrho_{32} - iG_c\varrho_{23}, \\ \partial_t\varrho_{21} &= -(i\Delta_p - i\Delta_c + \gamma_{21})\varrho_{21} - iG_p\varrho_{23} + iG_c\varrho_{31} + \gamma_{SGC}e^{-i\phi}\varrho_{33}, \\ \partial_t\varrho_{31} &= -(i\Delta_p + \gamma_{31})\varrho_{31} + iG_p(\varrho_{11} - \varrho_{33}) + iG_c\varrho_{21}, \\ \partial_t\varrho_{32} &= -(i\Delta_c + \gamma_{32})\varrho_{32} - iG_c(\varrho_{33} - \varrho_{22}) + iG_p\varrho_{12},\end{aligned} \tag{3}$$

with the conjugate relation $\varrho_{ij} = \varrho_{ji}^*$, $\varrho_{33} + \varrho_{22} + \varrho_{11} = 1$, and $\dot{\varrho}_{ij} = 0$ in the steady state. And In Eq. (3), $\gamma_{ij} = \left(\Gamma_i + \Gamma_j\right)/2$ represents the coherent relaxation rate between states $|i\rangle$ and $|j\rangle$. For this atomic model system, we have $\gamma_{32} = \gamma_{23} = (\Gamma_{31} + \Gamma_{32})/2$, $\gamma_{31} = \gamma_{13} = (\Gamma_{31} + \Gamma_{32} + \Lambda)/2$, and $\gamma_{21} = \gamma_{12} = \Lambda/2$. The analytical solution of ϱ_{31} in the steady state can be obtained by solving the density matrix equation ($\partial_t\varrho_{ij} = 0$) under the weak-field approximation, as follows:

$$\varrho_{31} = \frac{i\Omega_c^3 e^{i\phi}\Lambda\gamma_{\mathrm{SGC}}\left(\Gamma_{31} + \Gamma_{32}\right) + i\Omega_c^2\left[-\Lambda\Gamma_{32}\xi_{32} + \xi_{21}(\Lambda - \Gamma_{31})\left(\Gamma_{31} + \Gamma_{32}\right)\right]\Omega_p}{\left(\xi_{21}\xi_{31} + \Omega_c^2\right)\left[-\Lambda\Gamma_{32}\xi_{23}\xi_{32} + \left(2\Lambda + \Gamma_{31}\right)\left(\Gamma_{31} + \Gamma_{32}\right)\Omega_c^2\right]}, \tag{4}$$

with $\xi_{21} = -i\left(\Delta_p - \Delta_c\right) - \Lambda/2$, $\xi_{23} = i\Delta_c - \left(\Gamma_{31} + \Gamma_{32}\right)/2$, $\xi_{31} = -i\Delta_p - \left(\Gamma_{31} + \Gamma_{32} + \Lambda\right)/2$, and $\xi_{32} = -i\Delta_c - \left(\Gamma_{31} + \Gamma_{32}\right)/2$. The steady state probe susceptibility $\chi_p\left(x\right)$ of each filled lattice cell can be obtained as follows:

$$\chi_p(x) = \mathrm{Re}\left[\chi_p(x)\right] + \mathrm{Im}\left[\chi_p(x)\right] = \frac{N_x\left|\mathbf{d}_{13}\right|^2\varrho_{31}}{\varepsilon_0\hbar G_p}. \tag{5}$$

Here, $\mathrm{Re}\left[\chi_p(x)\right]$ and $\mathrm{Im}\left[\chi_p(x)\right]$ represent the real and imaginary parts of the susceptibility, corresponding to dispersion and absorption lines of the probe field, ε_0 is the dielectric constant in vacuum, and the spatial atomic density N_x, which can be considered as a Gaussian distribution in each filled lattice cell, is given by

$$N_x = \frac{N_0\lambda_0}{\delta_x\sqrt{2\pi}} \cdot e^{\left[-(x-x_0)^2/2\delta_x^2\right]}, \tag{6}$$

where N_0 is the average atomic density, x_0 is the trap center, $\delta_x = \lambda_{Lat}/(2\pi\sqrt{\eta})$ is the half-width with $\eta = 2U_0/(\kappa_B T)$ related to the capture depth U_0 and temperature T. $\lambda_0 = \lambda_{Lat}/2$ is the width

OPTICS CONTINUUM

of each cell, with λ_{Lat} being the wavelength of a red-detuned retroreflected laser beam forming the optical lattice. For the Bragg condition, the incident angle is given by $\alpha = \arccos(\lambda_p/\lambda_{Lat0})$, where λ_p is the wavelength of the probe field and $\lambda_{Lat0} = \lambda_{Lat} - \Delta\lambda_{Lat}$ with the geometric Bragg shift $\Delta\lambda_{Lat}$. It is worth emphasizing that the condition for trapping atoms is $\lambda_{Lat} > \lambda_{31}$ with λ_{31} being the wavelength of the transition $|3\rangle \leftrightarrow |1\rangle$. Here, we use the average susceptibility $\overline{\chi}_p = (N_0 |\mathbf{d}_{13}|^2 \varrho_{31})/(\varepsilon_0 \hbar G_p)$ to describe the propagation characteristics of the probe field.

The reflection and transmission properties of the defective lattice can be characterized by a 2×2 unimodular transfer matrix [67–69]. For filled lattice cells, we divide each cell into enough thin layers that can be regarded as a homogeneous medium. In general, the reflection coefficient depends in a complex way on the layer thickness for layers of finite size. However, the method of transfer matrix is valid in 1D atomic lattice for the transfer matrix of vacuum layer is unit. With the transfer matrix $m(x_j)$ of a single layer, we can obtain reflection coefficient $r_l(x_j) = -m(2,1)/m(2,2)[r_r(x_j) = m(1,2)/m(2,2)]$ on the left (right) side of this layer, depending on the Fresnel coefficients which are determined by the refractive index $n_f(x) = \sqrt{1 + \chi_p(x)}$. For the homogeneous and thin layer $r_l(x_j) = r_r(x_j) = r(x_j)$. Then $m(x_j)$ can be written as follows:

$$m(x_j) = \frac{1}{t(x_j)} \begin{bmatrix} t(x_j)^2 - r(x_j)^2 & r(x_j) \\ -r(x_j) & 1 \end{bmatrix}. \tag{7}$$

Here, $t(x_j)$ and $r(x_j)$ are the transmission and reflection coefficients of jth layer in each lattice cell with $j \in [1, 100]$. The transfer matrix of one filled cell can be expressed as follows:

$$M_f = \Pi_{j=1}^{100} m(x_j). \tag{8}$$

It is evident that this lattice exhibits the same reflectivities on both sides. The refractive index $n_v = 1$ for vacant lattice cells. Thus, the transfer matrix of a vacant cell can be written as follows:

$$M_v = \frac{1}{t(x)} \begin{bmatrix} t(x)^2 & 0 \\ 0 & 1 \end{bmatrix} = \begin{bmatrix} e^{ik_p\lambda_0} & 0 \\ 0 & e^{-ik_p\lambda_0} \end{bmatrix}, \tag{9}$$

with $k_p = 2\pi \cos\alpha/\lambda_p$. Then, the total transfer matrix is represented as follows:

$$M = (M_f)^{p_2} \cdot \left[(M_v)^{a_v} \cdot (M_f)^{a_f}\right]^{p_1}. \tag{10}$$

In further, we can calculate the reflection coefficient $r_l(r_r)$ on the left (right) of the lattice, which are given by

$$r_l = -\frac{M(2,1)}{M(2,2)}, r_r = \frac{M(1,2)}{M(2,2)}. \tag{11}$$

Here, $M(i,j)$ (where $i,j = 1,2$) denotes an element of the total transfer matrix M. The reflectivities on both sides of the one-dimensional defective atomic lattice can be obtained as follows:

$$R_l = |r_l|^2 = \left|-\frac{M(2,1)}{M(2,2)}\right|^2, \tag{12}$$

$$R_r = |r_r|^2 = \left|\frac{M(1,2)}{M(2,2)}\right|^2. \tag{13}$$

Thus, with the reflectivities of Eqs. (12) and (13), we can get the high reflection band in the Bragg condition:

$$\frac{\omega_p}{c}\left[p_1(a_f\lambda_0\overline{n_f(x)} + a_v\lambda_0 n_v) + p_2\lambda_0\overline{n_f(x)}\right] = k\pi, \tag{14}$$

where c is the speed of light in vacuum, k is an arbitrary positive integer, and $\overline{n_f(x)}$ is the average refractive index of a filled cell. The non-reciprocity between left and right reflectivities can be

OPTICS CONTINUUM

quantified by the contrast factor as follows:

$$C = \left|\frac{R_l - R_r}{R_l + R_r}\right|. \tag{15}$$

An important figure of merit to check the nonreciprocity. Obviously, the reasonable value of contrast satisfies the relation $0 \leq C \leq 1$ in an optical response system. If and only if $C = 0$, the left-side and right-side reflection are reciprocal, otherwise, they are nonreciprocal. And when $C \to 1$, almost perfect nonreciprocal reflection (unidirectional reflection) can be achieved.

3. Numerical results and discussions

In this section, we mainly discuss and optimize the process for nonreciprocal reflection amplification to unidirectional reflection amplification. At first, aiming to analyze the influence of SGC, the modulation of left and right reflections by the relative phases of laser fields ϕ and the angle between the two dipole moments θ should be checked, for ϕ and θ are all caused by the SGC effect, with the chosen parameters of defective atomic lattice $a_f = 1$, $a_v = 440$, $p_1 = 15$, and $p_2 = 12$. As shown in Figs. 2(a) – 2(d), there are significantly amplified nonreciprocal reflection peaks within the SGC ($\theta = \pi/3$), when ϕ is an even multiple of $\pi/2$ corresponding to double nonreciprocal reflection peaks, otherwise corresponding to single nonreciprocal reflection peak. It is worth noting that the reflectivity on the left side has almost reached $15,000$, while the reflectivity on the right side is almost 150. It seems that the intensity of the left and right reflections are modulated simultaneously by the relative phase, which hinges on the gain of the probe field. Therefore, we further analyze the modulation of average probe susceptibility by the relative phase of one period. Figure 2(e) clearly shows that there appear two gain peaks around $\phi = 0$, π, and 2π, although the gain amplitude is relatively weak for $\phi = 0$ and 2π. However, a single strong gain peak appears around $\phi = (1, 3)\pi/2$. It should be noted that the reflections are only amplified when the gain amplitude over 0.01 ($\left|\mathrm{Im}\overline{\chi}_p\right| > 1.0 \times 10^{-2}$). Thus, we can manipulate the intensity and position of nonreciprocal reflection bands freely by modulating the relative phase.

In further, under different electric dipole moment angles θ, we plot the imaginary part of the average susceptibility $\mathrm{Im}\overline{\chi}_p$ varying with the detuning Δ_p to examine and discuss the influence of SGC on probe gain as in Figs. 3(a) and 3(b). It is easy to see that although the probe light can be amplified by an incoherent pump without SGC, i.e., $\theta = \pi/2$, the quantum interference channel induced by spontaneous emission is suppressed in this case, resulting in a lower gain amplitude (lower than 0.01). This gain is insufficient to amplify the reflections [see Fig. 3(a)], since significant amplification requires $|\mathrm{Im}\overline{\chi}_p| > 1.0 \times 10^{-2}$. When the two dipole moments are non-orthogonal, the gain amplitude will be greatly increased and varies with θ [see Fig. 3(b)]. In particular, a wide single gain peak [$\theta \in (-\pi/2, \pi/2)$] can split into two narrow ones [$\theta \in (\pi/2, 3\pi/2)$] by modulating θ, and the gain amplitude lower than 0.01 around $\theta = \pi/2$ [see Fig. 3(c)], which is in good agreement with Figs. 2. The phenomenon where the gain is weakest at $\theta = \pi/2$ can also be explained from the the expression of ϱ_{31} in the Eq. (4). To simply and clearly illustrate the regulation of probe gain by θ, we set $\Delta_c = 0$, $\phi = \pi$, and $\Gamma_{31} = \Gamma_{32} = \gamma$, the imaginary part of the density matrix element $\mathrm{Im}[\varrho_{31}]$ at resonance ($\Delta_p = 0$) can be obtained as:

$$\mathrm{Im}[\varrho_{31}] = -\frac{4\Lambda\Omega_c^2\left[2\Omega_c\gamma\cos\theta + \Lambda\Omega_p\right]}{\left[\Lambda(2\gamma + \Lambda) + 4\Omega_c^2\right]\left[\gamma^2\Lambda + 2(\gamma + 2\Lambda)\Omega_c^2\right]} \tag{16}$$

From the above equation, it can be seen that the absorption (gain) spectrum is highly sensitive to θ, with the gain being proportional to $\cos\theta$. When $\theta \in (\pi/2, 3\pi/2)$, the probe field exhibits strong absorption at resonance, while for $\theta \in (-\pi/2, \pi/2)$, the probe field shows significant gain at resonance. However, the merging and splitting of the gain peaks can be understood from

OPTICS CONTINUUM

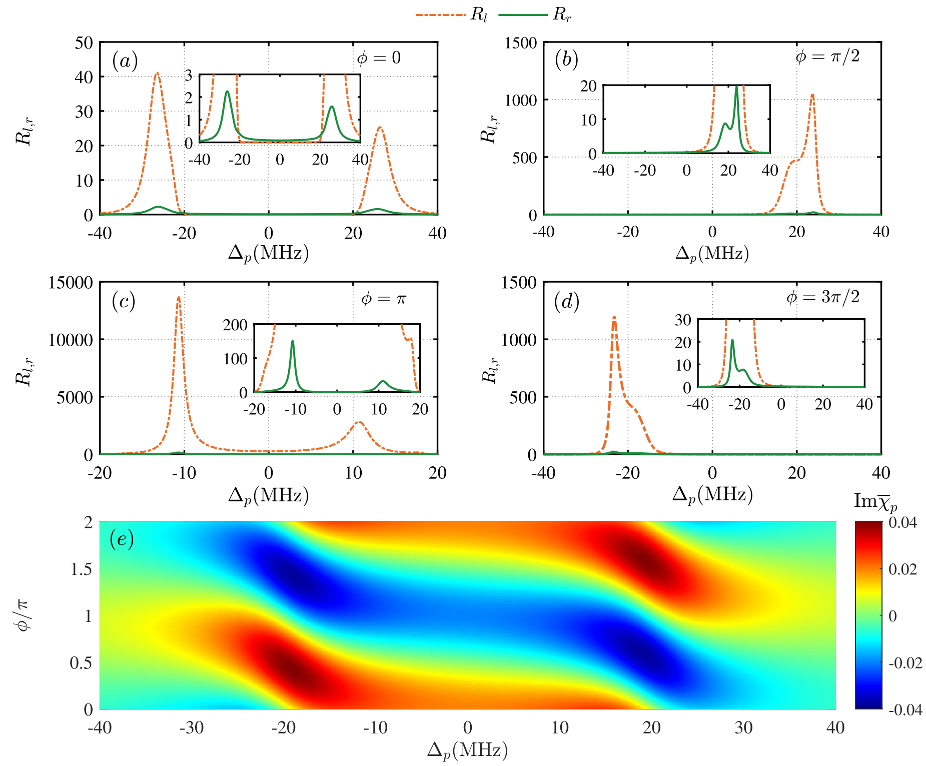

Fig. 2. (a), (b), (c), and (d) in different relative phases, the reflectivities $R_{l,r}$ *vs* detuning Δ_p. (e) The imaginary part of the average susceptibility $\mathrm{Im}\overline{\chi}_p$ *vs* detuning Δ_p and relative phase ϕ. The parameters: $\theta = \pi/3$, $a_f = 1$, $a_v = 440$, $p_1 = 15$, $p_2 = 12$, $G_c = 20$ MHz, $G_p = 0.3$ MHz, Λ = 5MHz, $\Delta_c = 0$, $\varepsilon_0 = 8.8541878 \times 10^{-12}$F·m^{-1}, $\eta = 5.0$, $N_0 = 4 \times 10^{11}$ cm^{-3}, $d_{13} = 1.7944 \times 10^{-29}$ C·m, $\Gamma_{31} = \Gamma_{32} = 5.75$MHz, $\lambda_{Lat} = 796.8$ nm, $\Delta\lambda_{Lat} = 0.9$ nm, and $\lambda_{31} = 794.978$ nm.

dressed-state theory. The strong coupling field splits the $|2\rangle$–$|3\rangle$ subsystem into two dressed states, producing two resonance branches in the probe response. The θ-dependent SGC mainly modifies the gain spectrum by redistributing the spectral weights and effective linewidths of these two branches. When $\theta \approx \pi/2$, the SGC is weak, so the distinction between the two branches is unclear and the peaks tend to be suppressed or merged. As θ moves away from $\pi/2$, the stronger SGC makes the double-peak structure more evident. This implies that the SGC effect not only increases the gain by two orders of magnitude but also enables accurate and flexible modulation of the amplified unidirectional reflection by adjusting the angle between the two dipole moments.

In the following, we will optimize the parameters of the defective atomic lattice to explore unidirectional reflection amplification. Although the peaks of the left and right reflections increase and decrease simultaneously. Notably, within the high-gain frequency region $\Delta_p \in (-6$ MHz, 6 MHz) [see inset in Fig. 2(c)], the left reflectivity exceeds 200, while the right reflectivity approaches zero. Focus on this frequency range, we set $\Delta_p = 0.3$ MHz with $\phi = \pi$ to examine the reflections and the contrast factor C *vs* the number of vacant lattice cells a_v in Fig. 4. With the increased a_v, the left and right reflectivities exhibit periodic oscillations that increase or decrease simultaneously [see Fig. 4(a)]. This can be explained by Eq. (14), the Bragg condition will be satisfied periodically with the variation of a_v. The noteworthy feature is that the left reflectivity

OPTICS CONTINUUM

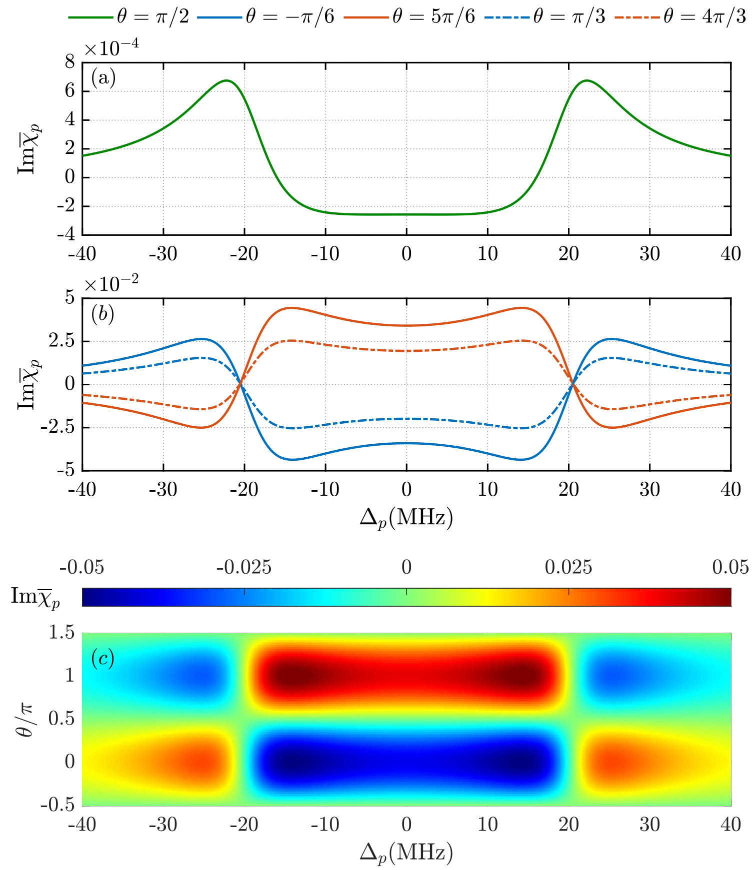

Fig. 3. (a), (b) The imaginary part of the average susceptibility $\mathrm{Im}\overline{\chi}_p$ *vs* detuning Δ_p at different angles θ of electric dipole moments. (c) The imaginary part of the average susceptibility $\mathrm{Im}\overline{\chi}_p$ *vs* detuning Δ_p and angle θ. Where $\phi = \pi$, other parameters are the same as in Fig 2.

is always more than 1, the right reflectivity can be reduced to 10^{-4} corresponding to the rather high contrast $C \simeq 1$ (0.9999995) [see Fig. 4(b)] for $a_v = 440$.

In Fig. 5, at the point $\Delta_p = -0.3$ MHz, we plot the left and right reflectivities, and the corresponding contrast factor C with the variation of filled lattice cells a_f, the number of periods of part I p_1 and part II p_2, respectively. Figures 5(a) and 5(b) show that the left and right reflectivities are reciprocal corresponding to the contrast $C = 0$ with $a_f = 0$, for the light response depends only on part II. When $a_f = 1$, the left reflectivity reaches its maximum value, corresponding to the right reflectivity reachs its minimum value, the perfect unidirectional reflection amplification can be achieved with $C \simeq 1$. It is clear that a ideal unidirectional reflection amplification can only be obtained in the regions $p_1 \in (10, 20)$ [see Figs. 5(c) and 5(d)] and $p_2 \in (0, 20)$ [see Figs. 5(e) and 5(f)], that the reflectivity on the right-side is lower than 1.0. Especially, the numerical results show that the amplified perfect unidirectional reflection appears at $a_f = 1$, $p_1 = 15$ and $p_2 = 12$, with the determined ϕ and θ.

Why are the reflectivities on the right and left sides so sensitive to the relative phase ϕ, the angle θ, and the lattice parameters a_v, a_f, p_1, and p_2? The physical essence is that the probe susceptibility can be modulated by ϕ and θ, which exhibits the optical response and determines the refractive index during the process of light propagation. In particular, the formation of a

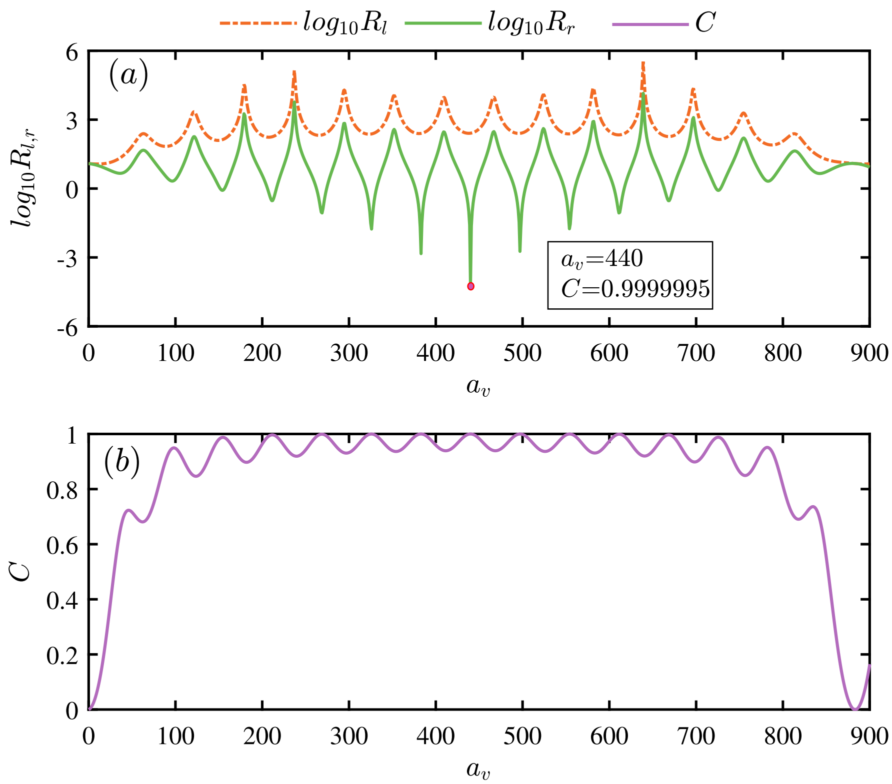

Fig. 4. (a) The logarithm of the reflectivities $log_{10}R_{l,r}$ *vs* vacant cells a_v. (b) The contrast factor C *vs* vacant cells a_v. Where $\phi = \pi$. $\Delta_p = -0.3$ MHz, and other parameters are the same as in Fig 2.

perfect reflection band requires meeting the Bragg condition, which depends on lattice parameters and the refractive index, as can be seen from Eq. (14). When the probe light incident from left side of the defective atomic lattice, the reflectivity mainly depends on part I, on the contrary, mainly depends on part II. Therefore, the left and right reflection bands maybe offset or overlapped depending on the Bragg condition, which can exhibit the nonreciprocity even unidirectionality.

Finally, we consider the modulation of nonreciprocal reflections by the coupling detuning Δ_c. The imaginary part of the average susceptibility in Fig. 6(a) clearly exhibits that a single gain peak first splits into double ones and then merges with the increased Δ_c, corresponding to $\Delta_c < -10$ MHz, $\Delta_c \in (-10$ MHz, 10 MHz), and $\Delta_c > 10$ MHz, respectively. Especially, the gain amplitude almost reaches 2.0×10^{-2} around the probe resonance point at $\Delta_c \in (-5$ MHz, 5 MHz). These well reflect the variation of left and right reflections with Δ_c as shown in Figs. 6(b) and 6(c), a single nonreciprocal reflection amplification band (region *I*) can split double ones (region *II*), and then merged into one (region *III*). In particular, an amplified unidirectional reflection band can be formed [corresponding to $\Delta_c \in (-5$ MHz, 5 MHz)] in region *II*. It is noticeable that the results in Fig. 6 are in good agreement with Fig. 2(c) when $\Delta_c = 0$. The modulation of the gain window position by the coupling field detuning Δ_c can be explained using dressed-state theory. From the physical mechanism perspective, the strong coupling field dresses the $|2\rangle - |3\rangle$ manifold and splits the probe response into two dressed-state resonance branches, whose approximate positions are given by

$$\Delta_p^{(\pm)} = \frac{\Delta_c \pm \sqrt{\Delta_c^2 + G_c^2}}{2}. \tag{17}$$

OPTICS CONTINUUM

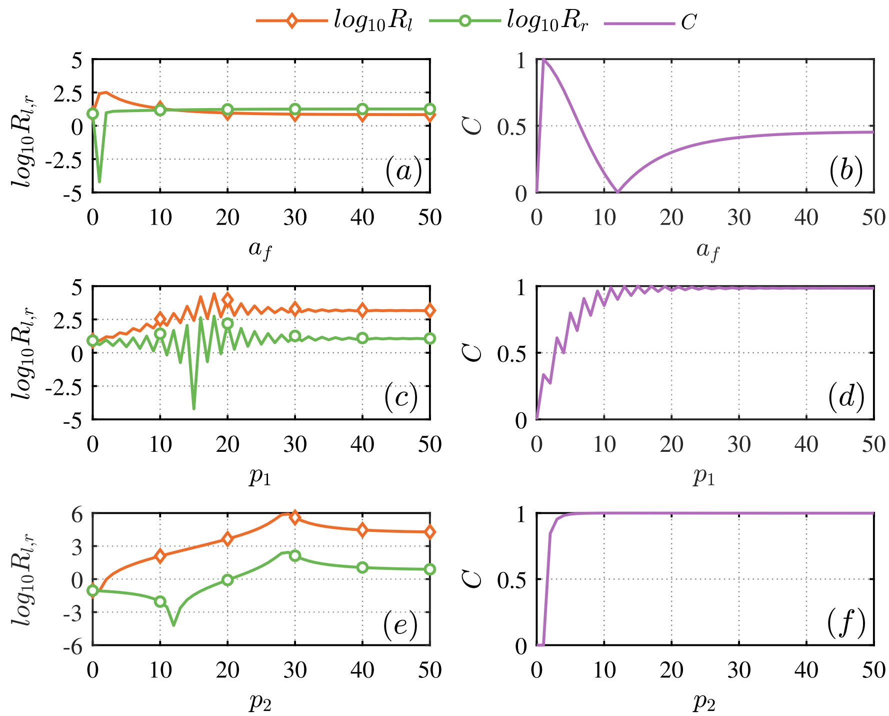

Fig. 5. (a), (c), and (e) show the logarithm of reflectivities $log_{10}R_{l,r}$ *vs* a_f, p_1, and p_2, respectively. (b), (d), and (f) show the contrast factor C *vs* a_f, p_1, and p_2, respectively . Here $p_1 = 15$, $p_2 = 12$ in (a)-(b), $p_2 = 12$, $a_f = 1$ in (c)-(d), and $p_1 = 15$, $a_f = 1$ in (e)-(f). Where $\phi = \pi$, $\Delta_p = -0.3$ MHz, and other parameters are the same as in Fig 2.

Therefore, varying Δ_c shifts the center of the gain window approximately along the Δ_p axis. Based on satisfying the gain condition, strong reflection also requires that the effective phase of the probe light in the lattice meets the Bragg condition. As a result, when both dressed-state branches overlap with the Bragg-matched spectral region, two reflection maxima can appear, corresponding to a double-peak response. When only one branch meets the Bragg condition, the spectrum evolves into a single-peak reflection. In summary, the frequency-tunable probe gain directly dictates the spectral positions of the amplified nonreciprocal or unidirectional reflection bands.

OPTICS CONTINUUM

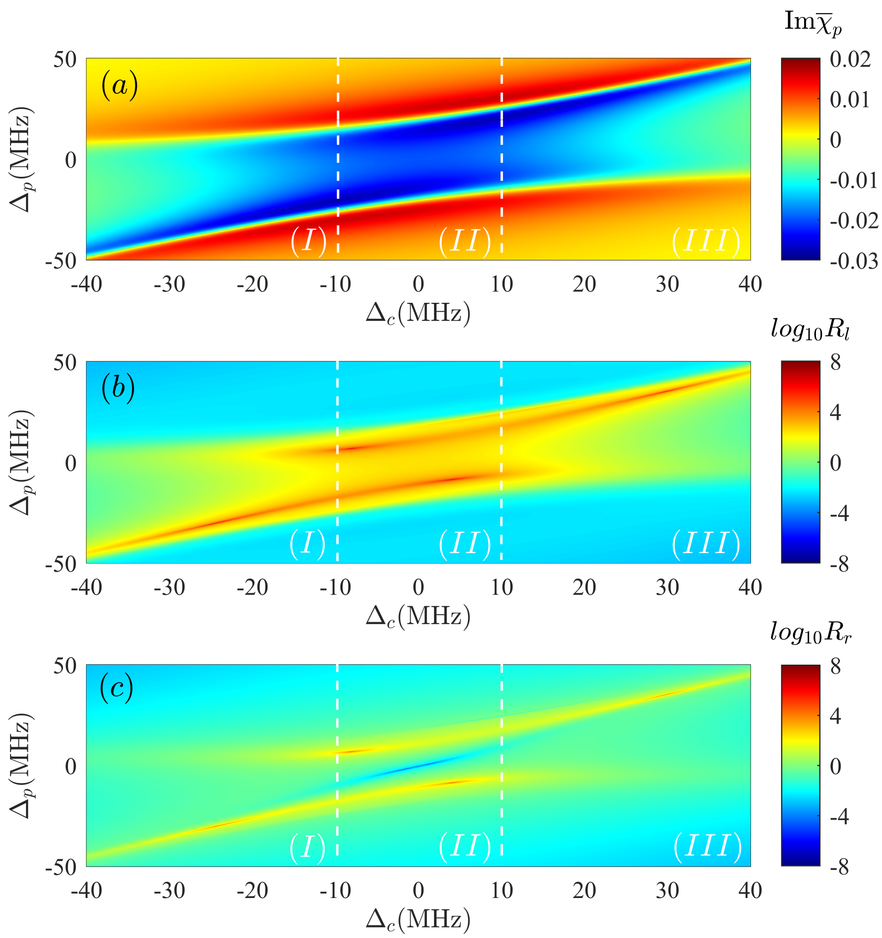

Fig. 6. (a), (b) and (c), respectively, the imaginary part of the average susceptibility Im$\overline{\chi}_p$ and the logarithm of the reflectivities $log_{10}R_{l,r}$ *vs* detuning Δ_p and detuning Δ_c. Where $\phi = \pi$ and other parameters are the same as in Fig 2.

4. Experimental feasibility

According to experimental Refs. [64–66], we design the corresponding experimental setup in Fig. 1(d). Specifically, we first cool the atoms by a magneto-optical trap (MOT) and confine them in a retroreflected optical dipole trap formed by a Ti:sapphire laser. Subsequently, atoms in pre-designated filled lattice cells are thermally expelled using the drive out lasing, creating vacant lattice cells and thus fabricating the defective atomic lattice. The coupling and incoherent pump beams are incident at a small angle, and the probe reflection can be detected by avalanche photodiodes. Notably, during the experiment, a small number of atoms may escape from or be absent from the filled lattice cells, a phenomenon that can be regarded as random fluctuations in atomic density. According to previous studies on disordered atomic lattices [70,71], when there are random fluctuations in atomic density, the main reflection features are usually quite robust, and the spectra generally exhibit only moderate changes, such as slight variations in peak height, bandwidth, or spectral position. Therefore, for realistic experimental situations, we expect that the main results of the present work remain qualitatively robust against weak and randomly distributed atom loss.

OPTICS CONTINUUM

5. Conclusions

In summary, we have explored SGC activated by a weak incoherent pump to attain gain-assisted nonreciprocal or even unidirectional reflection amplification in a three-level Lambda-type system of cold atoms trapped in an optical lattice. The atomic lattice (i.e., the optical lattice with trapped atoms) is designed to consist of two parts: part I with periodically vacant lattice cells, and part II with filled lattice cells. In our regime, the defective atomic lattice can not only break the spatial symmetry of probe susceptibility to achieve nonreciprocal reflection, but also make the probe light form amplified bandgaps through multiple reflections in the gain region assisted by the SGC. By adjusting the relative phase ϕ, the dipole moment angle θ, and the parameters of defective atomic lattice, e.g., the numbers of filled and vacant lattice cells in part I, the defect period in part I, and the period of filled lattice cells in part II, we have achieved the modulation from monochrome to two-color nonreciprocal reflection amplification, and even perfect unidirectional reflection amplification. In particular, the left reflectivity can be amplified by a factor of 250 (amplified by a factor of 250 relative to the incident intensity), while the right reflectivity is only 10^{-4}. These results stem from the combination of SGC-induced effects and Bragg conditions, which can provide potential avenues for implementing all-optical nonreciprocal devices that are widely used in integrated chips.

Funding. National Natural Science Foundation of China (12564048, 12204137, 12564047, 11874004, 11204019); Hainan Provincial Graduate Innovative Research Project (Qhys2024-402).

Disclosures. The authors declare no conflicts of interest.

Author Contributions

H.Y. conceived and designed the project. H.Y., Q.X. and C.P. wrote the original draft. Q.X., C.P. and D.C. prepared all figures. Q.X., C.P., H.Z. and D.Y. prepared for software. H.Y. wrote and edited the main manuscript. All authors reviewed the manuscript and agreed to the published version of the manuscript.

Data availability. No data were generated or analyzed in the presented research.

References

1. Y.-Q. Hu, Y.-H. Qi, Y. You, *et al.*, "Passive nonlinear optical isolators bypassing dynamic reciprocity," Phys. Rev. Appl. **16**(1), 014046 (2021).
2. H. Tian, J.-Q. Liu, A. Siddharth, *et al.*, "Magnetic-free silicon nitride integrated optical isolator," Nat. Photonics **15**(11), 828–836 (2021).
3. G. D'Aguanno, D. L. Sounas, H. M. Saied, *et al.*, "Nonlinearity-based circulator," Appl. Phys. Lett. **114**(18), 181102 (2019).
4. R. Navarathna, D. T. Le, A. R. Hamann, *et al.*, "Passive superconducting circulator on a chip," Phys. Rev. Lett. **130**(3), 037001 (2023).
5. P. Edinger, A. Y. Takabayashi, C. Errando-Herranz, *et al.*, "Silicon photonic microelectromechanical phase shifters for scalable programmable photonics," Opt. Lett. **46**(22), 5671–5674 (2021).
6. R. Karimian, S. Taravati, M. D. Ardakani, *et al.*, "Nonreciprocal-beam phased-array antennas based on transistor-loaded phase shifters," IEEE Trans. Antennas Propag. **69**(11), 7572–7581 (2021).
7. F. Lecocq, L. Ranzani, G. A. Peterson, *et al.*, "Nonreciprocal microwave signal processing with a field-programmable Josephson amplifier," Phys. Rev. Appl. **7**(2), 024028 (2017).
8. B. Ahmadi, P. Mazurek, P. Horodecki, *et al.*, "Nonreciprocal quantum batteries," Phys. Rev. Lett. **132**(21), 210402 (2024).
9. S.-C. Zhang, Y.-Q. Hu, G.-W. Lin, *et al.*, "Thermal-motion-induced non-reciprocal quantum optical system," Nat. Photonics **12**(12), 744–748 (2018).
10. Z.-Z. Wang, N. Xie, Z.-Y. Huang, *et al.*, "Propagation and amplification law of undetermined stray light and influence of signal-to-noise ratio in a multipass amplifier system," Opt. Lasers Eng. **169**, 107712 (2023).
11. J. Zhao, J. Dias, J.-Y. Haw, *et al.*, "Quantum enhancement of signal-to-noise ratio with a heralded linear amplifier," Optica **4**(11), 1421–1428 (2017).
12. N. Kuse and K. Minoshima, "Amplification and phase noise transfer of a Kerr microresonator soliton comb for low phase noise THz generation with a high signal-to-noise ratio," Opt. Express **30**(1), 318–325 (2022).
13. C. Krafczyk, A. N. Jordan, M. E. Goggin, *et al.*, "Enhanced weak-value amplification via photon recycling," Phys. Rev. Lett. **126**(22), 220801 (2021).
14. F. Lecocq, L. Ranzani, G. A. Peterson, *et al.*, "Efficient qubit measurement with a nonreciprocal microwave amplifier," Phys. Rev. Lett. **126**(2), 020502 (2021).
15. S. Taravati and G. V. Eleftheriades, "Full-duplex reflective beamsteering metasurface featuring magnetless nonreciprocal amplification," Nat. Commun. **12**(1), 4414 (2021).

16. Y.-W. Jing, H.-Q. Shi, and X.-W. Xu, "Nonreciprocal photon blockade and directional amplification in a spinning resonator coupled to a two-level atom," Phys. Rev. A **104**(3), 033707 (2021).
17. K.-W. Huang, Y. Wu, and L.-G. Si, "Parametric-amplification-induced nonreciprocal magnon laser," Opt. Lett. **47**(13), 3311–3314 (2022).
18. B. Peng, Ş. K. Özdemir, F. Lei, *et al.*, "Parity-time-symmetric whispering-gallery microcavities," Nat. Phys. **10**(5), 394–398 (2014).
19. L.-N. Song, Q. Zheng, X.-W. Xu, *et al.*, "Optimal unidirectional amplification induced by optical gain in optomechanical systems," Phys. Rev. A **100**(4), 043835 (2019).
20. S. Pucher, C. Liedl, S. Jin, *et al.*, "Atomic spin-controlled non-reciprocal Raman amplification of fibre-guided light," Nat. Photonics **16**(5), 380–383 (2022).
21. W. Zaets and K. Ando, "Optical waveguide isolator based on nonreciprocal loss/gain of amplifier covered by ferromagnetic layer," IEEE Photonics Technol. Lett. **11**(8), 1012–1014 (1999).
22. P. Liu, X.-Y. Zhang, X.-Z. Hao, *et al.*, "Stable directional amplification in one-dimensional non-Hermitian single-band systems," Phys. Rev. A **107**(5), 053515 (2023).
23. L.-X. Guo, L.-L. Wan, L.-G. Si, *et al.*, "Topological amplification and frequency conversion in a photonic lattice with a two-photon driving," Phys. Rev. A **108**(1), 013512 (2023).
24. N. T. Otterstrom, E. A. Kittlaus, S. Gertler, *et al.*, "Resonantly enhanced nonreciprocal silicon Brillouin amplifier," Optica **6**(9), 1117–1123 (2019).
25. L. Agazzi, J. D. B. Bradley, M. Dijkstra, *et al.*, "Monolithic integration of erbium-doped amplifiers with silicon-on-insulator waveguides," Opt. Express **18**(26), 27703–27711 (2010).
26. H. Park, A. W. Fang, O. Cohen, *et al.*, "A Hybrid AlGaInAs–silicon evanescent amplifier," IEEE Photonics Technol. Lett. **19**(4), 230–232 (2007).
27. E. S. Vyatkin and A. N. Poddubny, "Optomechanical amplification driven by interference of phonon-exciton and phonon-photon couplings," Phys. Rev. B **104**(7), 075447 (2021).
28. M. A. Cohen, D. Bothner, Y. M. Blanter, *et al.*, "Optomechanical microwave amplification without mechanical amplification," Phys. Rev. Appl. **13**(1), 014028 (2020).
29. R.-T. Sun, M.-Y. Peng, T.-X. Lu, *et al.*, "Multicolor nonreciprocal optical amplifier with spinning active optomechanics," Phys. Rev. A **109**(2), 023520 (2024).
30. J.-Q. Zhang, J.-X. Liu, H.-L. Zhang, *et al.*, "Topological optomechanical amplifier in synthetic PT-symmetry," Nanophotonics **11**(6), 1149–1158 (2022).
31. C.-S. Zhao, R. Peng, Z. Yang, *et al.*, "Nonreciprocal amplification in a cavity magnonics system," Phys. Rev. A **105**(2), 023709 (2022).
32. G.-W. Lin, S.-C. Zhang, Y.-Q. Hu, *et al.*, "Nonreciprocal amplification with four-level hot atoms," Phys. Rev. Lett. **123**(3), 033902 (2019).
33. L.-N. Song, Z.-H. Wang, and Y. Li, "Enhancing optical nonreciprocity by an atomic ensemble in two coupled cavities," Opt. Commun. **415**, 39–42 (2018).
34. Y. Zhang, Y.-M. Liu, T.-Y. Zheng, *et al.*, "Light reflector, amplifier, and splitter based on gain-assisted photonic band gaps," Phys. Rev. A **94**(1), 013836 (2016).
35. G.-R. Li, Y. Geng, X.-S. Pei, *et al.*, "Phase and detuning control of the unidirectional reflection amplification based on the broken spatial symmetry," Opt. Express **32**(7), 12839–12851 (2024).
36. Y. Geng, X.-S. Pei, G.-R. Li, *et al.*, "Spatial susceptibility modulation and controlled unidirectional reflection amplification via four-wave mixing," Opt. Express **31**(23), 38228–38239 (2023).
37. L. Jin, "Asymmetric lasing at spectral singularities," Phys. Rev. A **97**(3), 033840 (2018).
38. D. V. Novitsky, A. Karabchevsky, A. V. Lavrinenko, *et al.*, "PT symmetry breaking in multilayers with resonant loss and gain locks light propagation direction," Phys. Rev. B **98**(12), 125102 (2018).
39. T.-M. Li, H. Yang, M.-H. Wang, *et al.*, "Unidirectional photonic reflector using a defective atomic lattice," Phys. Rev. Res. **6**(2), 023122 (2024).
40. Q.-Y. Xu, G.-R. Li, Y.-T. Zheng, *et al.*, "Broadband unidirectional reflection amplification in a one-dimensional defective atomic lattice," Phys. Rev. A **110**(6), 063724 (2024).
41. T. Shui, W.-X. Yang, M.-T. Cheng, *et al.*, "Optical nonreciprocity and nonreciprocal photonic devices with directional four-wave mixing effect," Opt. Express **30**(4), 6284–6299 (2022).
42. D. Wang, W.-Q. Lu, J.-Y. Han, *et al.*, "Near-resonant twin-beam generation from degenerate four-wave mixing in hot ^{133}Cs vapor enabled by field-dressed energy levels," Opt. Express **31**(23), 38255–38267 (2023).
43. H.-M. Zhao, X.-J. Zhang, M. Artoni, *et al.*, "Nonlocal Rydberg enhancement for four-wave-mixing biphoton generation," Phys. Rev. A **109**(4), 043711 (2024).
44. H. Yang, T.-G. Zhang, and Y. Zhang, "Probe gain via four-wave mixing based on spontaneously generated coherence," Chin. Phys. B **26**(2), 024204 (2017).
45. L. N. Mai Anh, N. H. Bang, N. Van Phu, *et al.*, "Influence of spontaneously generated coherence on absorption, dispersion, and group index in a five-level cascade atomic system," Phys. Scr. **98**(4), 045106 (2023).
46. A. N. Nair and R. Arun, "Production and protection of entanglement via vacuum induced coherences," J. Phys. B: At. Mol. Opt. Phys. **57**(6), 065502 (2024).
47. M. Abbas, U. Saleem, Rahmatullah, *et al.*, "Spontaneously generated structured light in a coherently driven five-level M-type atomic system," Phys. Rev. A **109**(2), 023716 (2024).

48. R. Ahmad, H. Ali, I. Ahmad, *et al.*, "Spontaneously generated coherence in a four-level atomic system under induced chirality: Quantum control of the Casimir force," Results Phys. **46**, 106314 (2023).
49. M. Abbas, W. Z. Liu, Rahmatullah, *et al.*, "Spontaneously generated structured light," Phys. Lett. A **520**, 129727 (2024).
50. V. Moeini, S. H. Kazemi, and M. Mahmoudi, "Sub-Doppler laser cooling via spontaneous generated coherence," Laser Phys. **30**(2), 026001 (2020).
51. H. B. Crispin and R. Arun, "Squeezing in resonance fluorescence via vacuum induced coherences," J. Phys. B: At. Mol. Opt. Phys. **53**(5), 055402 (2020).
52. R. Hazra, R. Mukherjee, and N. Borgohain, "Spontaneously generated coherence (SGC) in a three-level V-type multiple quantum well nanostructures," AIP Conf. Proc. **3170**(1), 030001 (2024).
53. H. B. Crispin, "Simulating quantum interference effects in the fluorescence of a V-system with perpendicular dipole moments," J. Phys. B: At. Mol. Opt. Phys. **54**(7), 075402 (2021).
54. S.-C. Tian, Z.-H. Kang, C.-L. Wang, *et al.*, "Observation of spontaneously generated coherence on absorption in rubidium atomic beam," Opt. Commun. **285**(3), 294–299 (2012).
55. S.-C. Tian, R.-G. Wan, Z.-H. Kang, *et al.*, "Gain spectrum of a laser-driven tripod-type atom dynamically induced in the presence of spontaneously generated coherence," J. Opt. Soc. Am. B **29**(5), 881–890 (2012).
56. S.-C. Tian, C.-L. Wang, Z.-H. Kang, *et al.*, "Observation of linewidth narrowing due to a spontaneously generated coherence effect," Chin. Phys. B **21**(6), 064206 (2012).
57. Z.-M. Wu, J.-H. Li, and Y. Wu, "Vacuum-induced quantum-beat-enabled photon antibunching," Phys. Rev. A **108**(2), 023727 (2023).
58. Z.-M. Wu, J.-H. Li, and Y. Wu, "Phase-engineered photon correlations in weakly coupled nanofiber cavity QED," Phys. Rev. A **109**(3), 033709 (2024).
59. Z.-M. Wu, J.-H. Li, and Y. Wu, "Coherent perfect absorption accompanying subnatural narrowing by vacuum-induced coupling," Phys. Rev. A **110**(3), 033722 (2024).
60. H. S. Han, A. Lee, K. Sinha, *et al.*, "Observation of vacuum-induced collective quantum beats," Phys. Rev. Lett. **127**(7), 073604 (2021).
61. Y. Geng, C. Peng, X.-F. Zheng, *et al.*, "Unidirectional amplified reflections based on four-wave mixing and spontaneously generated coherence," Phys. Lett. A **534**, 130241 (2025).
62. J.-H. Wu and J.-Y. Gao, "Phase control of light amplification without inversion in a Λ system with spontaneously generated coherence," Phys. Rev. A **65**(6), 063807 (2002).
63. T. Shui, X.-M. Chen, and W.-X. Yang, "Coherent control of spatial and angular Goos–Hänchen shifts with spontaneously generated coherence and incoherent pumping," Appl. Opt. **61**(34), 10072–10079 (2022).
64. A. Schilke, C. Zimmermann, P. W. Courteille, *et al.*, "Photonic band gaps in one-dimensionally ordered cold atomic vapors," Phys. Rev. Lett. **106**(22), 223903 (2011).
65. A. Schilke, C. Zimmermann, and W. Guerin, "Photonic properties of one-dimensionally ordered cold atomic vapors under conditions of electromagnetically induced transparency," Phys. Rev. A **86**(2), 023809 (2012).
66. A. Schilke, C. Zimmermann, P. W. Courteille, *et al.*, "Optical parametric oscillation with distributed feedback in cold atoms," Nat. Photonics **6**(2), 101–104 (2012).
67. M. Artoni, G. C. La Rocca, and F. Bassani, "Resonantly absorbing one-dimensional photonic crystals," Phys. Rev. E **72**(4), 046604 (2005).
68. M. Artoni and G. C. La Rocca, "Optically tunable photonic stop bands in homogeneous absorbing media," Phys. Rev. Lett. **96**(7), 073905 (2006).
69. Y. Zhang, Y. Xue, G. Wang, *et al.*, "Steady optical spectra and light propagation dynamics in cold atomic samples with homogeneous or inhomogeneous densities," Opt. Express **19**(3), 2111–2119 (2011).
70. H. Yang, T. Zhang, Y. Zhang, *et al.*, "Dynamically tunable three-color reflections immune to disorder in optical lattices with trapped cold ^{87}Rb atoms," Phys. Rev. A **101**(5), 053856 (2020).
71. M. Wang, T. Li, Y. Zhang, *et al.*, "Three-color reflections in one-dimensional ordered and disordered atomic lattices with trapped N-type cold atoms," Opt. Express **30**(19), 34887–34897 (2022).